Validation of the Distribution of Stripping Loss Neutrals in the Accelerator of the Negative Ion Source

K. Ikeda,[1, a)] M. Kisaki,[1, 2] H. Nakano,[1, 2] K. Tsumori,[1, 2] K. Nagaoka,[1, 3] Y. Fujiwara,[1] S. Masaki,[2] E. Rattanawongnara,[2] and M. Osakabe[1, 2]

[1)] *National Institute for Fusion Science (NIFS), National Institutes of Natural Sciences, Toki, 509-5292, Japan*

[2)] *The Graduate University for Advanced Studies, SOKENDAI, Toki 509-5292, Japan*

[3)] *Graduate School of Science, Nagoya University, Nagoya 464-8603, Japan*

[a)] *Corresponding author: ikeda.katsunori@nifs.ac.jp*

Abstract. The difference of the stripping loss between hydrogen and deuterium is examined using two approaches. The first is the measurement of the optical beam emission. The wavelength of beam emission spectrum reflects the energy distribution of beam particles by the Doppler effect. The low-energy stripping peak is observed in the energy band corresponding to the extraction voltage, and also a moderate shoulder is distributed in the lower energy region. Secondly, the spatial and the energy distribution in the accelerator is estimated by the attenuation calculation using the vacuum pressure distribution in the accelerator. Stripping neutrals are concentrated in the low energy region, and a peak is formed at 9 keV in the energy distribution due to stripping neutrals inside the extraction grid aperture. The total stripping loss inside the accelerator is 16% for hydrogen and 24% for deuterium. The calculated Doppler-shifted spectra for hydrogen and deuterium clearly show the peak with the moderate shoulder on the redshift side, which is consistent with the measured results.

INTRODUCTION

Negative-ion based neutral beam injectors (N-NBI) are utilized for plasma heating and current drive in the Large Helical Device (LHD) [1, 2, 3]. The negative ion source is optimized for hydrogen operation which can outputted 40 A hydrogen negative ion current (I_{H^-}) [4, 5]. Hydrogen neutral beam power of 5 MW can be injected into the LHD vacuum vessel by an injector with two ion sources. Fusion plasma experiment with deuterium was initiated in 2017, and the N-NBI generated the deuterium beam by switching the operation gas without changing the ion source setting [6]. In the previous operation, the N-NBI generated the negative ion current of 55..4 A with the average current density of 223 A/m^3 which was 0.69 times the nominal hydrogen negative ion current (80 A) [7, 8]. The deuterium beam injection power was reduced to 2.9 MW, which was affected by neutralization and re-ionization reactions into the beam line and the reduction of negative ion current. A similar decrease in the deuterium negative ion current was also observed in the N-NBI in JT-60U [9]. The neutralization reaction also occurs inside the accelerator, which is called stripping loss in the case of a negative ion source because an electron is stripped from the negative ions. Stripping loss is one of the causes of the decrease in the output negative ion current, and its magnitude depends on the vacuum pressure distribution owing to the accelerator structure. In order to keep the stripping loss below 30% in deuterium operation, the maximum pressure of the ion source is set to be 0.3 Pa, which is also an important consideration in the design of the RF negative ion source for the N-NBI in ITER [10, 11]. Although stripping loss for hydrogen operation had not been a major problem in the N-NBI in LHD, understanding the increase in stripping loss in deuterium operations is necessary for efficient operation of the ion source. In addition, secondary electrons are generated at the location of the stripping neutrals, therefore the distribution of stripping neutrals helps to study the heat load reduction of the grid system.

In this paper, we report on the distribution of stripping loss neutral in the accelerator of N-NBI in LHD. Stripping neutrals have intermediate energies in the accelerator. We show the Balmer-α emission spectrum from a stripped hydrogen and deuterium neutral beam observed by Doppler beam emission spectroscopy. Next, beam neutralization was calculated by the vacuum pressure distribution inside the accelerator, which was derived from the simplified electrode structure. We also show the energy distribution of stripping neutrals which is consistent with the observed Doppler shifted beam emission spectrum. Finally, the effect on the negative ion current being extracted is discussed.

OBSERVATION BEAM EMISSION SPECTRUM

The N-NBI uses an arc discharge type high-current negative ion source, which is optimized for hydrogen operation in LHD. Figure 1 shows a cross-sectional view of the accelerator for the negative ion source in the beam line number 3 (BL3). Hydrogen negative ions are generated on the surface of the plasma grid (PG) covered with a thin layer of Cs and are extracted into the accelerator using the potential difference of 10 kV with the extraction grid (EG). The PG and the EG have 770 apertures. The negative ions are accelerated with a potential difference of 170 kV between EG and grounded grid (GG), and 770 beamlets are ejected from 55 slots in the GG. In the accelerator, stripped neutrals are generated by the collision between the hydrogen negative ion beam and hydrogen gas molecules ($H^- + H_2 \rightarrow H + H_2 + e$). The energy of neutrals are fixed at the production point which are not accelerated any further. Therefore, the negative ion beam emitted from the GG contains stripped neutrals with energy less than full energy. An optical device to observe visible light emission from stripped neutrals was installed in a downstream vacuum chamber as shown in Fig. 1. The line of sight (LOS) was set up for the angle of $\theta = 33^\circ$ to the center axis of the neutral beam. The collected light was injected into a spectrometer with the focal length of 25 cm by a quartz optical fiber. An intensified charge couple detector (ICCD) was used to detect the Doppler shifted spectrum with an averaged wavelength resolution of 0.21 nm/pixel. The Doppler-shifted wavelength λ_d is given by

$$\lambda_d = \lambda_0(1 - \beta cos\theta), \tag{1}$$

where λ_0 and θ are the wavelength of emitted light emission and the observation angle, respectively. The β is defined by $\beta = v/c$ where v and c are the particle speed and the light speed, respectively. In the case of Balmer-α emission, the wavelength of Doppler shift of 180 keV beam for hydrogen (H_α : 656.3 nm) and deuterium (D_α : 656.1 nm) are 10.7 nm and 7.6 nm, respectively. Therefore, the Doppler shift spectrum is possible to observe using this system. However, the non-shifted spectrum cannot be separated because the difference in wavelength between H_α and D_α is 0.2 nm which is the same as the system resolution.

Figure 2 shows the beam emission spectrum from hydrogen (dotted line) and deuterium (bold line) in the 171 keV beam operation with the extraction voltage of 9 kV. Intense full-energy peaks were observed at 646 nm for hydrogen and 649 nm for deuterium. The unshifted peaks of the background are located at the wavelengths of H_α and D_α. The peak in the stripping spectrum is located near the unshifted peak and the stripped energy corresponds to the energy of the extraction voltage. However, there is no stripping peak in the accelerated energy band.

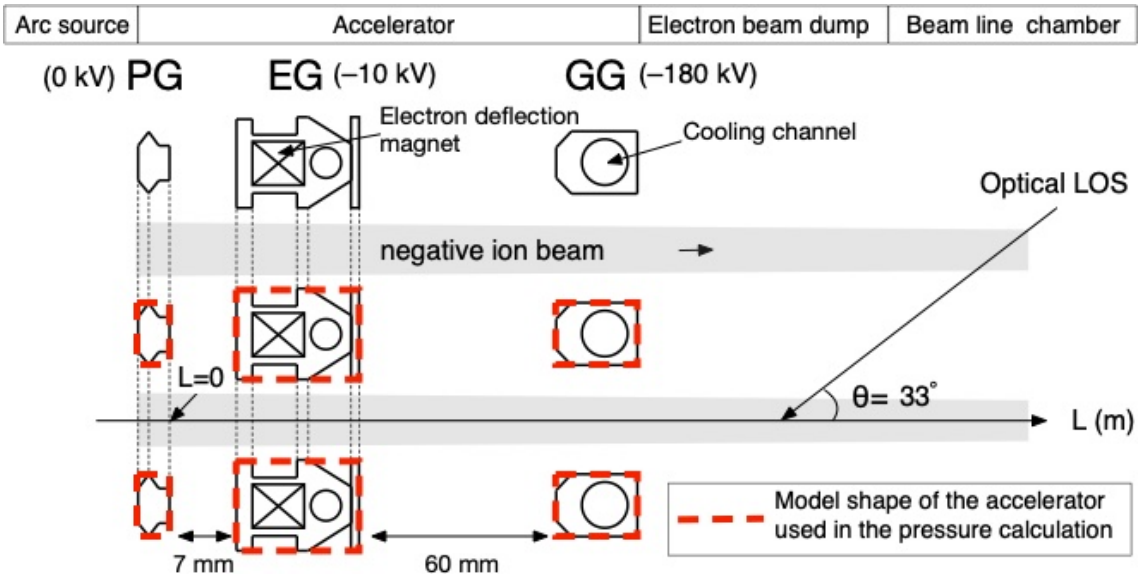

FIGURE 1. The cross-sectional drawing of the beam accelerator of the negative ion source in the N-NBI (BL3) in LHD. The optical line of sight to observed beam emission H_α is set 33° to the center of beam line.

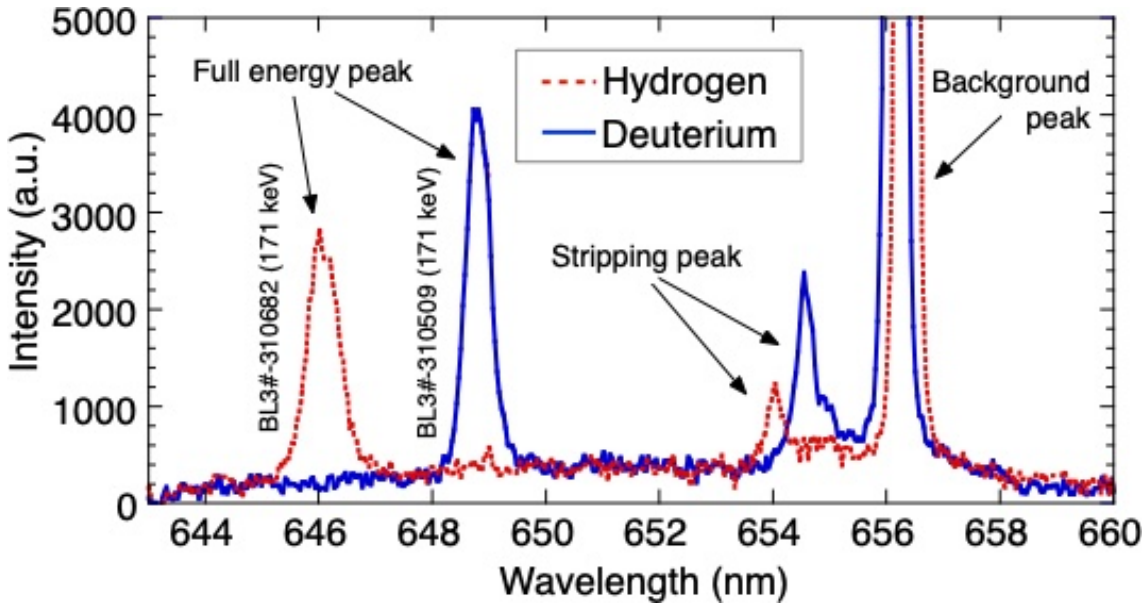

FIGURE 2. The Doppler shifted beam emission spectra of hydrogen (dotted line) and deuterium (bold line) appear on the blueshift side of the non-shifted background spectrum from the ion source. The peaks from full energy (171 keV) beam and stripping neutrals on the low energy position are observed.

BEAM STRIPPING CALCULATION

In order to confirm the beam stripping inside the accelerator, the negative ion decay was calculated. The procedure is as follows. i) A simplified structure of the accelerator model was constructed with the appropriate aperture size in the grid system. ii) A positional distribution of neutralization and re-ionization cross-section were obtained by a published reaction database. iii) A positional distribution and an energy distribution of stripped neutrals were obtained by calculation of beam attenuation. Then, a Doppler-shifted spectrum was estimated from the energy distribution of stripped neutrals and an emission cross-section of Balmer-α.

A simplified accelerator model, shown as a dotted line in Figure 1, which was used to obtain the vacuum pressure distribution. The aperture shapes and sizes of each grid are shown in Table 1. The PG aperture is a simple circle with a diameter of 14 mm, and an aperture depth is 4 mm. The EG aperture is also a circle shape with a diameter of 10 mm, and its aperture depth is 14 mm. The number of EG and GG apertures is 770. The GG has a slot structure with a width of 14 mm and a longitudinal size of 260 mm. The depth of the slot is 10 mm. The number of GG slots is 55. An electron beam dump is installed downstream of the ion source to remove residual electrons from the accelerator. The opening area is approximately the same as the total beam size and the length is 1.9 m. From these sizes, the conductance coefficients using H_2 and D_2 gas were obtained. Here, the molecular temperature was set at room temperature (300 K). Assuming an average pressure of 0.2 Pa in the EG approximated by a cylindrical tube, the average free path of molecular hydrogen is 33 mm. The Knudsen number K_n is 3.3 which is reasonable the molecular flow. Therefore, the flow in the accelerator was assumed to be a molecular flow. The conductance coefficient C_{20air} for air using an ideal orifice of zero thickness and opening area A is $C_{20air} = 116A$ (at 20°C, air). The conductance C_{mol} for a gas with molecule mass number M and temperature T is converted to $C_{mol} = K\sqrt{28.8/M}\sqrt{T/293.15}C_{20air}$. Here, the K is the the shape factor referenced by Guthrie [12] for a cylindrical tube and Dushman [13] for square shape. The conductances of each grid were derived for the hydrogen and deuterium cases by using the model shapes shown in Table 1. The total system conductance of the accelerator C_{tot} is $C_{tot}(H)$ = 6.9 m^3/s for hydrogen and $C_{tot}(D)$ = 4.9 m^3/s for deuterium. The throughput Q for the accelerator is constant at each position and can be determined from the differential pressure ΔP between the filling gas pressure of the arc chamber and the vacuum pressure in the downstream vessel ($Q = C_{tot}\Delta P$). In hydrogen and deuterium beam operations, the filling gas pressure in the arc chamber was set to 0.3 Pa and 0.43 Pa, respectively. The equivalent pressure in the downstream vacuum vessel was 0.02 Pa in both cases. Additional hydrogen gas was supplied to the neutralization cell in hydrogen beam operation; however no additional deuterium gas was supplied to the neutralization cell to maintain the neutralization efficiency

TABLE I. Dimensions of a simplified accelerator model grid to estimate the vacuum distribution. The PG and the EG consist of multi-apertures, and the GG is set multi-slots configuration. An electron beam dump is installed between the accelerator and the downstream vacuum chamber.

Parts	Opening shape	Material	Opening size	Depth	Quantity
PG	aperture	Mo	14 mm (diameter)	4 mm	770
EG	aperture	Cu	10 mm (diameter)	14 mm	770
GG	slot	Cu	260 mm × 14 mm	10 mm	55
Electron beam dump	rectangle	Cu	265 mm × 1190 mm	1900 mm	1

in deuterium beam operation. Using these vacuum pressures, the throughput is $Q(H)$ = 1.9 Pa·m^3/s for hydrogen and $Q(D)$ = 2.0 Pa·m^3/s for deuterium. Figure 3 shows the vacuum pressure distribution inside the accelerator, which was solved from this throughput using the conductance of each grid. The horizontal axis is the distance L from the PG back surface, and the shadow areas are the PG and the EG. The right end of the Fig. 3 is the surface of the GG. The vacuum pressure decreases downstream to approximately 0.1 Pa in the acceleration region between EG and GG. The single-dotted line in Figure 3 is the energy of the particles in the accelerator. The extraction voltage and the acceleration voltage are 9 kV and 162 kV, respectively. Here, the beam energy is assumed to be linear increasing. However, the actual potential curve on the center axis of the beamlet is not linear near the surface of grid because the electric field seeps into the aperture [4], which is one of the reasons for the widening of the stripping peak. However, it does not significantly affect the total number of stripping neutrals and the location of the stripping peak.

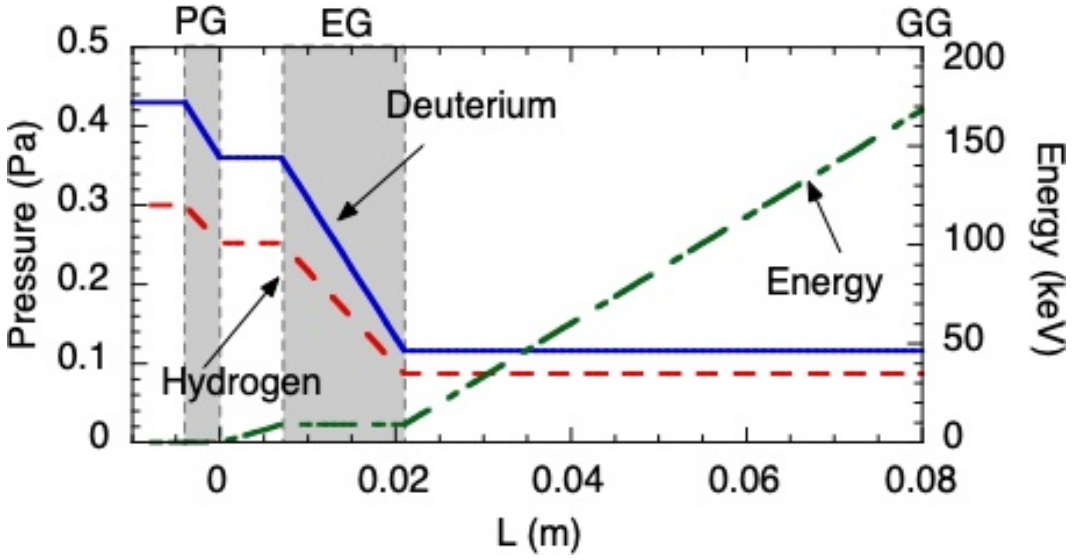

FIGURE 3. Vacuum pressure distribution estimated by the modeled accelerator and one-dimensional calculations, where L is the distance from the back surface of the PG. The hydrogen (bold line) and deuterium (dashed line) pressure in the arc chamber was 0.3 Pa and 0.43 Pa, respectively. The downstream vacuum vessel pressure was 0.02 Pa measured at beam operation. Neutralized gas was used in the hydrogen operation, and was not used in the deuterium operation. The single-dotted line shows the assumed energy distribution used in the calculation.

The ratio of beam particles to background molecules is shown here. Assuming an average pressure of 0.2 Pa at the EG position, the molecular hydrogen density n_{H_2} inside the EG aperture is $n_{H_2} = 4.8 \times 10^{19}$ m^{-3}. On the other hand, considering a maximum H$^-$ current of 40 A passes through the EG, the averaged H$^-$ current density at the EG location is 662 A/m^2 based on the size and number of EG apertures shown in Table 1. The velocity of H$^-$ with the energy of 9 keV passed through the EG is 1.3×10^6 m/s. The density of H$^-$ beam (n_{beam}) is $n_{beam} = 3.3 \times 10^{15}$ m^{-3}. Therefore, the number density of the beam is very small compared to the background molecular density ($n_{beam}/n_{H_2} = 6.9 \times 10^{-5}$). During the actual beam operation, decrease in downstream vacuum pressure was not observed during the beam extraction. Therefore, the following beam attenuation calculations were performed under the condition that the vacuum pressure in the accelerator does not change during beam extraction.

Before calculating the negative ion decay inside the accelerator, the spatial distribution of the neutralization cross-section σ_n was determined by the Oak Ridge National Laboratory database [14]. The main reaction of neutralization is the collision between negative ions and gas molecules ($H^- + H_2 \rightarrow H + H_2 + e$), and the cross-section data for F8 [14] was selected as shown in Fig. 4(a). The bold line and the dashed line are deuterium and hydrogen, respectively. The neutralization cross-section is described by the energy of the particles. Here, the cross-section of deuterium was defined as the cross-section of hydrogen with the same velocity. The σ_n exceeds 1×10^{-15} cm^2 for negative ion energies below 10 keV. However, the σ_n decreases as the beam energy is increased. The σ_n of deuterium is larger than that of hydrogen above 5 keV. Figure 4(b) shows the spatial distribution of the neutralization cross-section using the particle energy distribution inside the accelerator (see in Fig. 3). The large σ_n is maintained in the interval from PG to EG, and the cross-section decreases in the acceleration region with increasing beam energy. The σ_n for deuterium is large in the vicinity of EG which is supposed to be the reason for the large stripping loss in deuterium operation compared to hydrogen.

In the accelerator, the neutralized beam is converted into positive ions through a re-ionization reaction by collision with molecular hydrogen ($H + H_2 \rightarrow H^+ + H_2 + e$). The cross-section σ_r was derived from the database E6 [14]. The maximum σ_r is 1.5×10^{-16} cm^2 for 30 keV hydrogen which is one order smaller than the neutralization cross-section. The negative ion decay is calculated in the small section of dL = 1 mm, and the reaction in the volume in one section is written by $N(mol) \times N(neg) \times \sigma_n \times dL$ and $N(mol) \times N(neu) \times \sigma_r \times dL$ for neutralization and re-ionization, respectively. Here, $N(neg)$ and $N(neu)$ is the number of negative ions and neutral particles, respectively, and the number of molecule $N(mol)$ was obtained from Boltzmann's constant, pressure and room temperature in this calculation.

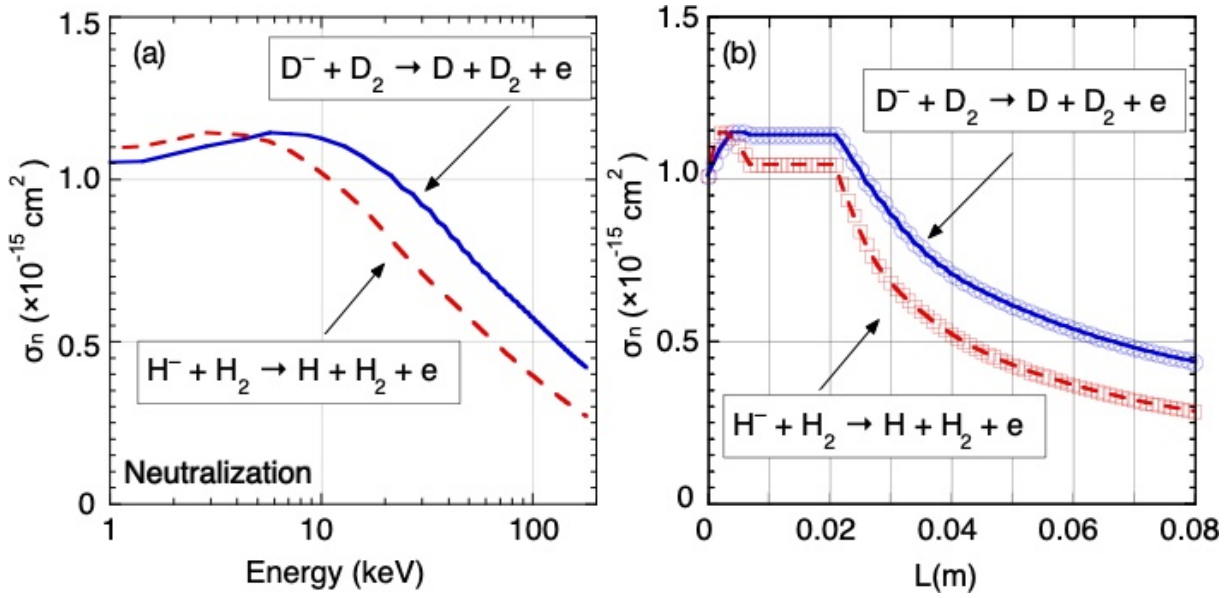

FIGURE 4. Energy distribution (a) and spatial distribution (b) of the neutralization cross-sections of hydrogen (dashed line) and deuterium (bold line) inside the accelerator. The reaction cross-section is referred from the Oak Ridge National Laboratory database [14]

Figure 5(a) shows the distribution of neutrals which is the amount of the subtraction from the number of neutralized particles and the number of re-ionized particles. The bold line and the dashed line are deuterium and hydrogen, respectively. The neutralization peak occurs between the PG and the EG, which have high molecular density and high neutralization cross-section, with peak values of 0.7% and 0.95% for hydrogen and deuterium, respectively. The re-ionization peak is also located at the same position; however the re-ionization positive ions are negligibly small peaks of 0.015% and 0.033% for hydrogen and deuterium, respectively. The total number of the neutrals produced in the accelerator is as low as 16% in hydrogen operation, but it increases to 24% in deuterium. Figure 5(b) shows the energy distribution of neutrals in the accelerator. The energy distribution forms a sharp peak at 9 keV in both hydrogen and deuterium, which is due to a neutralization reaction inside the apertures in the 14 mm thick EG. The neutrals with 9 keV extraction energy are 6% and 9% for hydrogen and deuterium, respectively, and these neutrals account for 37% of the stripping neutrals. The energy distribution of stripping neutral is asymmetric and the number

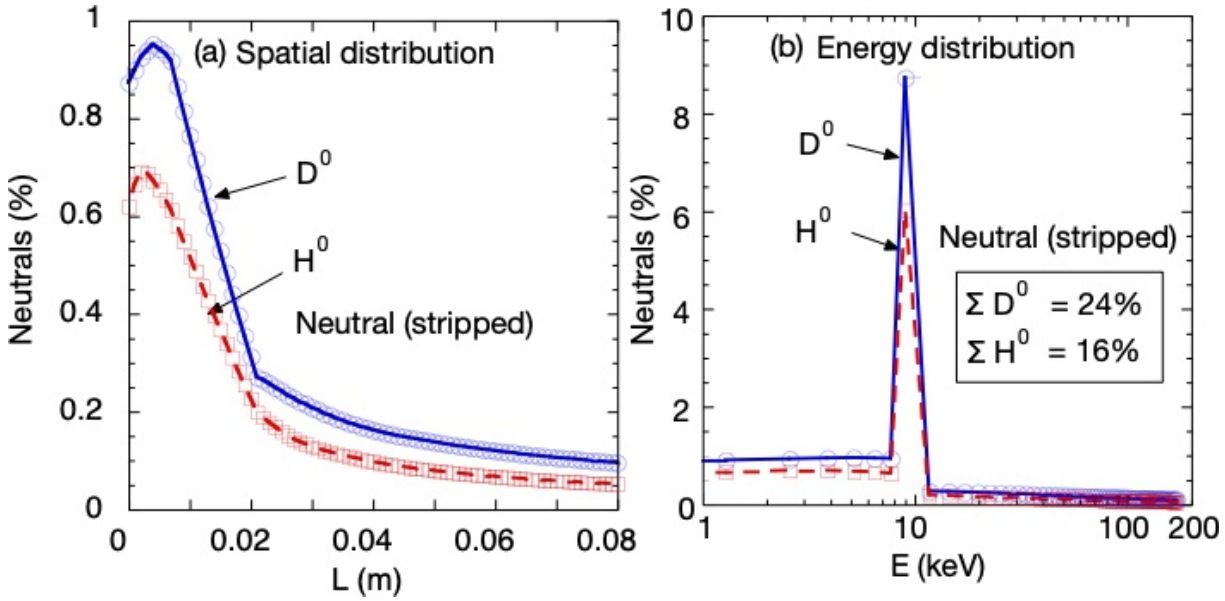

FIGURE 5. Spatial distribution (a) and energy distribution (b) of stripping neutrals generated from a hydrogen (dashed line) and deuterium (bold line) negative ion beam.

of stripping neutrals per unit of energy in the acceleration region is smaller than the number of stripping neutrals in the extraction region. The stripped hydrogen neutrals ejected from the accelerator are excited by the collision with a hydrogen molecular, and it emits the H_α light ($H + H_2 \rightarrow H + H_2 + H_\alpha$). Therefore, the Doppler-shifted H_α light spectrum can be estimated from the energy distribution of the neutrals. The reaction cross-sections for the emission of the Balmer lines σ_e are based on C12 in the cross-section database [14]. The reaction cross-section is approximately $\sigma_e = 1 \times 10^{-17}$ cm^2 for 10 keV hydrogen.

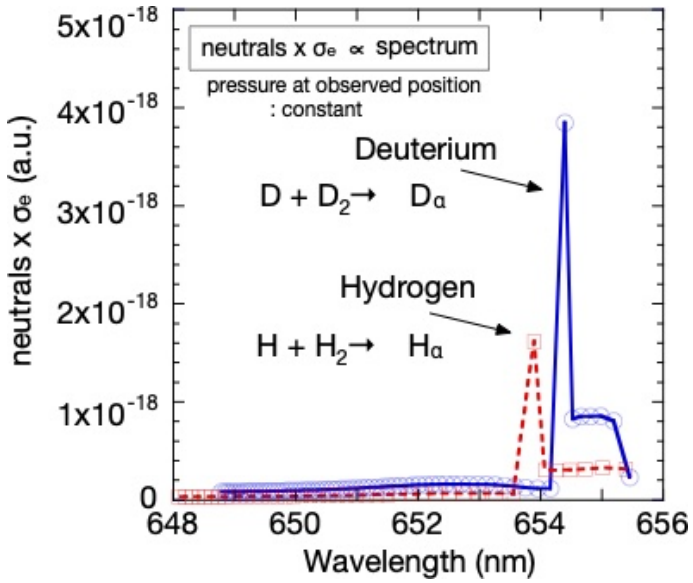

FIGURE 6. Doppler shifted spectrum obtained from stripped neutral particles and beam emission cross-sections, where the gas molecular density at the observation point is assumed to be equal for hydrogen (dashed line) and deuterium (bold line).

The emission intensity of H_α is proportional to the product of $\sigma_e \times N(mol) \times N(neu)$. Here, spectrum intensity I_{DS} is defined $I_{DS} = \sigma_e \times N(neu)$ because the vacuum pressure is the same for hydrogen and deuterium at the observation

position. The amount of Doppler shift wavelength is obtained from the speed of stripping neutrals as shown in Eq. (1). Figure 6 shows the calculated Doppler shifted H_α and D_α spectra emitted from the stripped neutrals extracted from the accelerator. The peak of the 9 keV extraction energy (see in Fig. 5(b)) clearly appears on the blue-shift side of the Balmer-α line as a stripping loss peak due to the Doppler effect. The deuterium stripping peak is 2.3 times larger than the hydrogen stripping peak because the intensity of the spectral peak is greatly affected by the stripping loss neutrals. The observed stripping peak for deuterium was higher than that for hydrogen peak (see in Fig. 2), which is in good agreement with the estimated Doppler shift spectrum. The calculated spectra also clearly shows that the spectral intensity due to the stripping loss in the acceleration region (EG - GG) is very small. It is difficult to measure the broad and small stripping components in the acceleration region using this diagnostic, therefore we cannot observe these small stripping spectra as shown in Fig. 2. On the other hand, a moderate shoulder clearly appears on the red-shift side of the stripping peak in the calculations. The intensity of moderate shoulder is approximately 20% of the stripping peak which also appeared in the measured Doppler shifted spectrum as shown in Fig 2. In the actual measurement, the peak widths widen depending on the width of the monochromator, beamlet divergence, and inclination of the grids. Therefore, the peak intensity decreases and widens the spectrum, and large shoulders should appear. From these calculations, the moderate shoulder on the red-shift side of the stripping peak is due to the stripping losses in the low energy region between the PG and the EG.

In this connection, several factors should be discussed in combination for the output negative ion current. It had been reported that the density of negative ions produced in the ion source increased in the deuterium discharge. Although the surface negative ion density cannot be measured with the LHD-NBI source, the deuterium negative ion density was 1-1.3 times higher than the hydrogen negative ion density in the 1/3-sized negative ion source (RINS) in NIFS [7, 15]. The negative ion density in the vicinity of the PG was strongly affected by the operational conditions such as arc discharge power and surface Cs coverage. If the negative ion extraction follows the Child-Langmuir law, the extraction factor of negative ion should be 1 and 0.7 for hydrogen and deuterium, respectively. The residual fraction of negative ions due to stripping loss is estimated to be 0.84 and 0.76 for hydrogen and deuterium, respectively. Combining these factors gives an output factor of 0.84 for the negative ion current in hydrogen, and the output factor for deuterium to be in the range of 0.53 - 0.69. Therefore, the output negative ion current ratio I_{D^-}/I_{H^-} is considered to be between 0.63 and 0.82. The output negative ion current ratio of the LHD-NBI is approximately 0.69, which is considered to be within the range of the calculated I_{D^-}/I_{H^-}.

CONCLUSION

The stripping loss in the negative ion source of the LHD NBI is confirmed to be 16% for hydrogen and 24% for deuterium. In the deuterium operation, the operating gas pressure is increased to 0.43 Pa to suppress the electron current at high arc power discharge. However, the low stripping loss of less than 30% was maintained. The low stripping loss is due to the high transparency slot-type GG which maintains a low vacuum pressure condition in the acceleration region between EG and GG. The experimental value of the current ratio of $I_{D^-}/I_{H^-} = 0.69$ is consistent within the expected range (0.63 - 0.82) which is calculated stripping efficiency, the negative ion density ratio in the RNIS ion source and the negative ion extraction efficiency. To increase the output negative ion current, it is necessary to improve the negative ion density in the source or to improve the extraction efficiency by optimizing the extraction voltage. On the other hand, stripping neutrals with the extraction energy produced inside the EG aperture reach 37% of the total stripping loss. The calculated energy spectrum is in good agreement with the Doppler-shifted spectra measured by the beam emission spectroscopy. Therefore, the stripping calculation using a simplified grid model is considered to be correct. Especially, the moderate shoulder distributed on the red-shift side of the asymmetric stripping peak is well reproduced by this stripping calculation, which shoulder consists of low-energy neutral component produced between PG and EG. This result shows that not only low operating gas pressure but also a thin EG are effective in reducing stripping loss.

ACKNOWLEDGMENTS

The authors would like to thanks the technical staffs of NBI in LHD. This research is supported by the budget for the NIFS No. ULRR702.

REFERENCES

1. A. Iiyoshi, A. Komori, A. Ejiri, M. Emoto, H. Funaba, M. Goto, K. Ida, H. Idei, S. Inagaki, et al., Nucl. Fusion **39**, 1245 (1999).
2. O. Kaneko, Y. Takeiri, K. Tsumori, Y. Oka, M. Osakabe, K. Ikeda, K. Nagaoka, T. Kawamoto, E. Asano, and M. Sato, Nucl. Fusion **43**, 692 (2003).
3. T. Mutoh, K. Nagaoka, H. Takahashi, H. Kasahara, M. Osakabe, S. Kubo, T. Shimozuma, et al., Fusion Science and Technology **68**, 216 (2015).
4. Y. Takeiri, O. Kaneko, K. Tsumori, Y. Oka, M. Osakabe, K. Ikeda, E. Asano, T. Kawamoto, and R. Akiyama, Rev. Sci. Instrum. **71**, 1225 (2000).
5. K. Tsumori, K. Nagaoka, M. Osakabe, Y. Takeiri, K. Ikeda, O. Kaneko, Y. Oka, T. Kawamoto, et al., Rev. Sci. Instrum. **75**, 1847 (2004).
6. K. Ikeda, K. Tsumori, M. Kisaki, H. Nakano, K. Nagaoka, M. Osakabe, S. Kamio, Y. Fujiwara, Y. Haba and Y. Takeiri, AIP Conference Proceedings **2011**, 060002 (2018).
7. K. Ikeda, K. Tsumori, H. Nakano, M. Kisaki, K. Nagaoka, S. Kamio,Y. Fujiwara,Y. Haba and M. Osakabe, Nucl. Fusion **59**, 076009 (2019).
8. K. Ikeda, K. Tsumori, K. Nagaoka, H. Nakano, M. Kisaki, Y. Fujiwara, S. Kamio, Y. Haba, S. Masaki, and M. Osakabe, Rev. Sci. Instrum. **90**, 113322 (2019).
9. Y. Okumura, Y. Fujiwara, M. Kashiwagi, T. Kitagawa, K. Miyamoto, T. Morishita, M. Hanada, T. Takayanagi, M. Taniguchi, and K. Watanabe, Rev. Sci. Instrum. **71**, 1219 (2000).
10. R. Hemsworth, A. Tanga, and V. Antoni, Rev. Sci. Instrum. **79**, 02C109 (2008).
11. U. Fantz, P. Franzen, D. Wünderlich, Chemical Physics **398**, 7-16 (2012).
12. A. Guthrie and R. K. Wakerling, Vacuum equipment and techniques, McGraw-Hill (1949).
13. S. Dushman, Scientific foundations of vacuum technique ; 2nd Edition revised by J.M. Lafferty, John Wiley & Sons Inc (1962).
14. C. F. Barnett, Collisions of H, H_2, He and Li Atoms and Ions with Atoms and Molecules Atomic Data for Fusion, Volume 1, ORNL-6080, June (1990).
15. H. Nakano, M. Kisaki, K. Ikeda, K. Tsumori, K. Nagaoka, Y. Haba, S. Masaki, Y. Fujiwara, S. Kamio, and M. Osakabe, Jpn. J. Appl. Phys. **59**, SHHC09 (2020).